

Anomalous tunneling conductance in 2D metallic junctions with Rashba spin-orbit coupling and magnetization

Daisuke Oshima,¹ Katsuhisa Taguchi,¹ and Yukio Tanaka¹

¹*Department of Applied Physics, Nagoya University, Nagoya, 464-8603, Japan*

A metal with both Rashba type spin-orbit coupling (RSOC) and exchange coupling, which we call Ferromagnetic Rashba metal (FRM) has nontrivial metallic states, *i.e.*, normal Rashba metal (NRM), anomalous Rashba Metal (ARM) and Rashba ring metal (RRM), and they are manipulated by tuning Fermi level via an applied gate voltage. We theoretically study tunneling conductance (G) in a normal metal/FRM junction by changing Fermi level due to an applied gate voltage V_g on FRM. We find wide variety of V_g -dependence of G , which depends on the three types of metallic state in FRM. In case of NRM, V_g -dependence of G is conventional. On the other hand, in case of ARM, where the Fermi level crosses only one of the spin-split bands, V_g -dependence of G becomes similar to that in conventional one(two)-dimensional system for the large (small) RSOC. Besides, in case of RRM, when the Fermi level locates at the lower branch of the spin-split band for large RSOC, V_g -dependence of the G is similar to that in one-dimensional normal metal junction. These anomalous properties stem from the spin-momentum locking of RSOC rather than the density of states in ARM, and RRM due to the strong RSOC. Hence, these features can open the next-generation of the spintronics via these metallic state, which is made by the large RSOC and exchange coupling.

I. INTRODUCTION

Charge transport in the presence of both spin-orbit coupling, and magnetization or applied magnetic field is an intriguing topic in the field of spintronics¹⁻¹². Rashba type spin-orbit coupling (RSOC), which has a potential promising control of charge transport, has properties of spin-momentum locking and of breaking the spin degeneracy of the energy bands. The former properties become prominent on a surface of topological insulators¹³⁻¹⁵. On the other hand, the latter properties directly reflect on the charge transport in tunneling junctions¹⁶⁻²⁵.

A metallic junction with a RSOC provides an intriguing tunneling conductance, which depends on an applied gate voltage (V_g), namely the position of the Fermi level^{21,24,25}. The V_g dependence of charge conductance $G(V_g)$ is determined whether the Fermi level crosses two spin-split bands E_+ and E_- , or only E_- [see in Fig 1(a)]. Since the resulting G is phenomenologically understood by the product of density of state (DOS) of left and right materials in the junction^{26,27}, $G(V_g)$ reflects on V_g -dependence of the DOS²⁴.

Simultaneous existing of RSOC and the exchange coupling (M) generate three types of metallic states. We dubbed this metallic system as ferromagnetic Rashba metal (FRM). These three states have different spin configurations at the Fermi surface. (i) The first case appears when the Fermi level crosses the two bands $E_{\pm}(k) = \hbar^2 k^2/(2m^*) \pm \sqrt{\alpha^2 k^2 + M^2}$, where α is the coefficient of the RSOC and m^* is an effective mass. In this case, it is known that there are inner and outer spin-dependent Fermi surfaces as shown in Fig.1(d). The spin polarization of the inner and outer Fermi surfaces are opposite direction in each angle³. We call it normal Rashba metal (NRM). (ii) The second one is realized when the Fermi level only crosses the E_- band. The number of spin split Fermi surface becomes one as shown in Fig.1(b)-(c)

and Fig.1(e). This state is named as anomalous Rashba metal (ARM)¹⁰. (iii) The third one occurs when Fermi level locates below $E_-(\mathbf{k} = 0)$. We call this state Rashba ring metal (RRM). In RRM, spin polarization of the inner and outer rings are the same direction, unlike the Fermi surface in NRM.

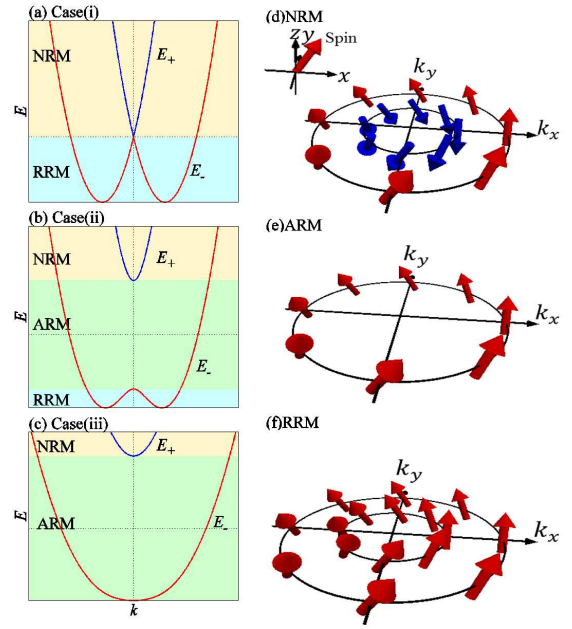


FIG. 1. (Color Online) The spin-split energy dispersion of the FRM in (a) $M = 0$, (b) $0 < M < 2E_\alpha$, and (c) $M \geq 2E_\alpha$, where $E_\alpha = m^* \alpha^2 / (2\hbar^2)$ and M denote the Rashba energy and exchange coupling, respectively. The yellow, green, and blue regions correspond to NRM, ARM, and RRM, respectively. ARM appears when $2E_\alpha > M$ is satisfied. The Fermi surface in these metallic states is illustrated in (d)-(f), where the arrows denote the spin-polarization at each \mathbf{k} .

Remarkably, the shape of the Fermi surface in the

RRM is different from that in the NRM as well as ARM: The shapes of the Fermi surface in RRM and NRM are ring-shape and disk-shape, respectively. Therefore, these energy dependence of the density of state (DOS) is dramatically difference from each other, and they could affect physical phenomena. It should be noted that in the presence of magnetization, RRM appears in the case that the energy scale of the RSOC is larger than that of M [see Fig. 1(b) and (c)]. Although the presence of the RRM requires the system to host a large RSOC, recent experiment has been reported two-dimensional systems with the large RSOC and magnetization, e.g., heterostructure of Pt/Co/Al-oxides²⁸. Therefore, RRM and ARM state in a FRM could be realized by tuning Fermi level with an applied gate voltage in thin layered hetrostructures.

In this paper, we study gate-voltage dependence of the tunneling conductance $G(V_g)$ in two-dimensional normal metal(NM)/FRM tunneling junction, when the magnetization of the FRM is along the out-of plane direction. We find wide varieties of the V_g -dependence of the conductance in NRM, ARM, and RRM. In particular, although we are studying two-dimensional (2D) system, the obtained results in ARM, and RRM become similar to those in conventional one-dimensional (1D) system. We expect that the anomalous properties stem from the spin-momentum locking of RSOC rather than the DOS in ARM and RRM. We also discuss how this phenomena can be detected experimentally by using a thin layered heterostructure like Pt/Co/Al-oxides. It is surprising that one-dimensional-like features emerge in the 2D junctions by tuning the Fermi level. These features can open the next-generation of the spintronics via RSOCs.

The organization of this paper is as follows. In Sec. II, we present a model of the NM/FRM junctions, and way to calculate $G(V_g)$. In Sec. III, to explain the origin of the anomalous V_g -dependence, we discuss systematic change of the Fermi surface and the DOS in NRM, ARM, and RRM. In Sec. IV, we summarize the results, and discuss a way to experimentally detect the anomalous tunneling conductance.

II. TUNNELING CONDUCTANCE IN NM/FRM JUNCTIONS

A. Model

We consider the tunneling conductance G in a NM/FRM junctions. In FRM region (right-side of the junction), both RSOC and exchange coupling exist: We assume that nonzero RSOC is generated by inversion symmetry breaking along the out-of plane direction due to an internal,²⁸ or an external electric field of the applied gate-voltage V_g ²⁹. Exchange coupling M is caused by the magnetization, which is along the out of plane direction. The Fermi level in FRM can be tuned by using the applied gate-voltage V_g . Since this paper defines that Fermi level E_F is measured from the bottom of the band

in the NM (left-side of the junction), V_g plays a role to shift the spin split energy band in FRM E_{\pm} , as illustrated in Fig. 2. This gate-voltage is assumed to affect only the FRM. On the other hand, in the left-side of the junction, RSOC, M and V_g are absent. At the interface between NM and FRM, a delta-function type tunneling barrier is assumed. It is also supposed that the interface is ideally flat-interface and the y -component of momentum of the wave function is conserved.

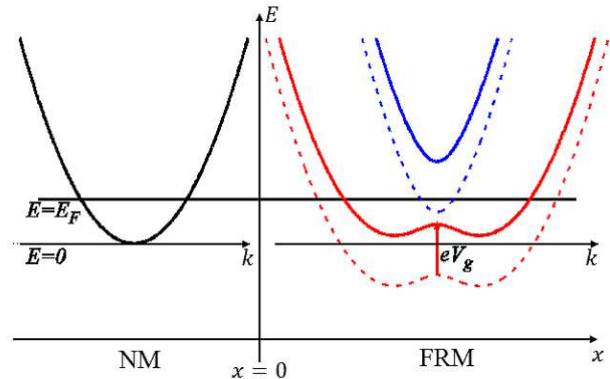


FIG. 2. (Color Online) The energy dispersion of the NM (left panel) and FRM (right panel) in the NR/FRM junction. We define that Fermi level E_F is measured from the bottom of the dispersion of the NM. In the presence of the gate voltage V_g in the FRM, the Fermi level of the FRM is shifted by V_g . In other words, the energy band dispersion (dashed lines) in the absence of V_g changes into the bold lines.

The model Hamiltonian in the junction can be described as

$$H = H_0\theta(-x) + U\delta(x) + H_{\text{FRM}}\theta(x), \quad (1)$$

where θ and δ are the Heaviside step function and delta-function, respectively. The first term in Eq. 1 shows left-side of the junction ($x < 0$) and denotes kinetic energy as $H_0 = \hbar^2 k^2 / (2m^*)$ with $\mathbf{k} = (k_x, k_y)$, $k^2 = k_x^2 + k_y^2$, and effective mass m^* of the NM. The second term $U\delta(x)$ indicates the tunneling barrier. U is the strength of tunneling barrier. The third term H_{FRM} expresses the effective Hamiltonian of FRM in the right-side of the junction ($x > 0$). H_{FRM} is given by^{3,10,30,31}

$$H_{\text{FRM}} = H_0 + \alpha(\mathbf{k} \times \boldsymbol{\sigma})_z - M\sigma_z + eV_g. \quad (2)$$

Here, the second term in Eq. (2) denotes the RSOC. α is the strength of the RSOC. The third term $M\sigma_z$ shows the exchange coupling. $\boldsymbol{\sigma}$ is Pauli matrices in spin space. The fourth term $eV_g (\geq 0)$ indicates the electrostatic potential caused by the gate-voltage in the right-side, where $e (> 0)$ is an elementary charge of an electron. The relation between V_g and the energy band of FRM are described in Fig. 2(b). Without loss of generality, we assume that the effective mass in each side are equal, and we set $\hbar^2 / (2m^*) = 1\text{eV}\text{\AA}$, $\alpha > 0$, and $M \geq 0$.

B. Tunneling conductance

From Eq. (2), we obtain the wave function in the left-side of the junction $\psi^{\uparrow(\downarrow)}(x < 0, y)$. Hereafter, the superscript \uparrow (\downarrow) denotes the up(down)-spin injection. $\psi^{\uparrow(\downarrow)}(x < 0, y)$ is decomposed into the injected wave function $\psi_{\text{in}}^{\uparrow(\downarrow)}$, and reflected one $\psi_{\text{ref}}^{\uparrow(\downarrow)}$ as

$$\psi^{\uparrow(\downarrow)}(x < 0, y) = \psi_{\text{in}}^{\uparrow(\downarrow)} + \psi_{\text{ref}}^{\uparrow(\downarrow)}, \quad (3)$$

$$\psi_{\text{in}}^{\uparrow} = e^{i(k_x x + k_y y)} \begin{pmatrix} 1 \\ 0 \end{pmatrix}, \quad \psi_{\text{in}}^{\downarrow} = e^{i(k_x x + k_y y)} \begin{pmatrix} 0 \\ 1 \end{pmatrix}, \quad (4)$$

$$\psi_{\text{ref}}^{\uparrow(\downarrow)} = e^{i(-k_x x + k_y y)} \begin{pmatrix} r_{\uparrow}^{\uparrow(\downarrow)} \\ r_{\downarrow}^{\uparrow(\downarrow)} \end{pmatrix}, \quad (5)$$

with $k_x = k \cos \phi$ and $k_y = k \sin \phi$. Here, $k = \sqrt{2m^*E}/\hbar$ and $\phi = \tan^{-1}(k_y/k_x)$ are the momentum of the electron in $x < 0$ and the angle between \mathbf{k} and the x -axis, respectively. $r_{\uparrow}^{\uparrow(\downarrow)}$ [$r_{\downarrow}^{\uparrow(\downarrow)}$] is the reflection coefficient of up[down]-spin electron with up(down)-spin injection, and it includes the spin-flip process.

Next, we consider the transmitted wave function. In the presence of both RSOC and magnetization, it should be noted that the eigenfunction for the eigenvalue of E_{\pm} at each energy are changed at $\Delta \equiv E - eV_g + E_c = 0$, as shown in Fig. 3. As a result, the transmitted wave function $\psi^{\uparrow(\downarrow)}(x > 0, y) \equiv \psi_{\text{tra}}^{\uparrow(\downarrow)}$ is characterized by Δ as

$$\psi_{\text{tra}}^{\uparrow(\downarrow)} = t_1^{\uparrow(\downarrow)} [\theta(\Delta)\phi_+(\mathbf{k}_1) + \theta(-\Delta)\phi_-(\mathbf{k}_1)] + t_2^{\uparrow(\downarrow)} \phi_-(\mathbf{k}_2),$$

with

$$\phi_+(\mathbf{k}) = e^{i\mathbf{k}\cdot\mathbf{r}} \begin{pmatrix} g_-(\mathbf{k}) \\ h(\mathbf{k}) \end{pmatrix}, \quad \phi_-(\mathbf{k}) = e^{i\mathbf{k}\cdot\mathbf{r}} \begin{pmatrix} h(\mathbf{k}) \\ g_+(\mathbf{k}) \end{pmatrix}. \quad (6)$$

Here, $t_1^{\uparrow(\downarrow)}$ [$t_2^{\uparrow(\downarrow)}$] denotes the transmission coefficient with up (down)-spin injection. $\mathbf{k}_1 = (k_{1,x}, k_y)$ and $\mathbf{k}_2 = (k_{2,x}, k_y)$ are the momentum in FRM, which are defined $k_1^2 < k_2^2$ [see Fig. 3(a)]. ϕ_{\pm} is the eigenfunction for the eigenvalue E_{\pm} . We set $g_{\pm}(\mathbf{k}_{1(2)}) = -ai(k_{1(2),x} \pm ik_y)$, and $h(k_{1(2)}) = M + \sqrt{\alpha^2 k_{1(2)}^2 + M^2}$. From the energy dispersion $E_{\pm}(k)$ with the condition $k_1^2 \leq k_2^2$, the magnitude of the momentum $k_{1(2)} = \sqrt{k_{1(2),x}^2 + k_y^2}$ is given by

$$k_{1(2)}^2 = \frac{2m^*}{\hbar^2} \left[(E - eV_g) + 2E_{\alpha} - (+)\sqrt{4E_{\alpha}(E - eV_g) + 4E_{\alpha}^2 + M^2} \right]. \quad (7)$$

To obtain k_1 and k_2 , we consider the velocity operator v_x . Since an electron is injected along $+x$ direction, the sign of the velocity v_x should take positive value, where the velocity in the FRM $v_x = \partial H/(\hbar \partial k_x)$ is given from Eq. (2) as^{3,21}

$$v_x = \frac{\hbar k_x}{m^*} + \frac{\alpha}{\hbar} \theta(x) \sigma_y. \quad (8)$$

TABLE I. Origin of the momentum of transmitted wave k_1 and k_2 for NRM, ARM, and RRM. Here, Δ equals to $E - eV_g + E_c$.

| State | E_+ | E_- |
|----------------------|-------------------|--------------------------|
| NRM | k_1 | k_2 |
| ARM [$\Delta > 0$] | k_1 (Imaginary) | k_2 |
| ARM [$\Delta < 0$] | – | k_1 (Imaginary), k_2 |
| RRM | – | k_1, k_2 |

Besides, it is noted that in ARM, k_1^2 takes negative value at each Fermi level, as shown in Fig. 3(b). Hence, k_1 becomes a pure imaginary. The sign of k_1 is determined so that $\phi_{\pm} \rightarrow 0$ in the limit of $x \rightarrow \infty$. The short summary of k_1 and k_2 of each metallic state is represented in Table I.

To solve the wave function, we consider the boundary condition at the interface^{10,16,21,24,32}:

$$\begin{aligned} \psi^{\uparrow(\downarrow)}(+0, y) - \psi^{\uparrow(\downarrow)}(-0, y) &= 0, \\ v_x [\psi^{\uparrow(\downarrow)}(+0, y) - \psi^{\uparrow(\downarrow)}(-0, y)] &= \frac{2U}{i\hbar} \psi^{\uparrow(\downarrow)}(0, y). \end{aligned} \quad (9)$$

Then, we obtain the probability current density $j_x(k_y) = \text{Re}[\psi^{\uparrow(\downarrow)\dagger} v_x \psi^{\uparrow(\downarrow)}]$ ^{21,24,32}, the reflection probability $R^{\uparrow(\downarrow)}$, and the transmission probability $T^{\uparrow(\downarrow)}$ given by

$$\begin{aligned} R^{\uparrow(\downarrow)}(k_y) &= \left| \frac{j_{x,\text{ref}}^{\uparrow(\downarrow)}}{j_{x,\text{in}}^{\uparrow(\downarrow)}} \right| = \text{Re} \left[\frac{\psi_{\text{ref}}^{\uparrow(\downarrow)\dagger} v_x \psi_{\text{ref}}^{\uparrow(\downarrow)}}{\psi_{\text{in}}^{\uparrow(\downarrow)\dagger} v_x \psi_{\text{in}}^{\uparrow(\downarrow)}} \right], \\ T^{\uparrow(\downarrow)}(k_y) &= \left| \frac{j_{x,\text{tra}}^{\uparrow(\downarrow)}}{j_{x,\text{in}}^{\uparrow(\downarrow)}} \right| = \text{Re} \left[\frac{\psi_{\text{tra}}^{\uparrow(\downarrow)\dagger} v_x \psi_{\text{tra}}^{\uparrow(\downarrow)}}{\psi_{\text{in}}^{\uparrow(\downarrow)\dagger} v_x \psi_{\text{in}}^{\uparrow(\downarrow)}} \right]. \end{aligned} \quad (10)$$

Here, $j_{x,\text{in}}^{\uparrow(\downarrow)}$, $j_{x,\text{ref}}^{\uparrow(\downarrow)}$, and $j_{x,\text{tra}}^{\uparrow(\downarrow)}$ are the x -component of injected, reflected, and transmitted probability current density, respectively. From $R^{\uparrow(\downarrow)}(k_y) + T^{\uparrow(\downarrow)}(k_y) = 1$, we can obtain $T^{\uparrow(\downarrow)}$ as

$$T^{\uparrow(\downarrow)}(k_y) = 1 - \left(|r_{\uparrow}^{\uparrow(\downarrow)}|^2 + |r_{\downarrow}^{\uparrow(\downarrow)}|^2 \right). \quad (11)$$

Finally, at the low temperature limit, the electric current I from left-side to right-side is given as follow^{21,24,33}:

$$\begin{aligned} I &= \frac{e}{2\pi\hbar} \int_{-\infty}^{\infty} dE \sum_{k_y(E,\phi)} \left[T^{\uparrow}(k_y) + T^{\downarrow}(k_y) \right] \\ &\quad \times [f(E, E_F + eV) - f(E, E_F)] \\ &\approx \frac{e^2 V L}{4\pi^2 \hbar} \int_{-\pi/2}^{\pi/2} d\phi \cos \phi k_F [T^{\uparrow}(E_F, \phi) + T^{\downarrow}(E_F, \phi)], \end{aligned} \quad (12)$$

where $k_F = \sqrt{2m^*E_F}/\hbar$, $f(E, E_F)$, and L are the Fermi momentum in the NM, the Fermi distribution function, and the width of the junction along the y direction, respectively. V is the applied voltage between the NM and FRM. The tunneling conductance per unit width,

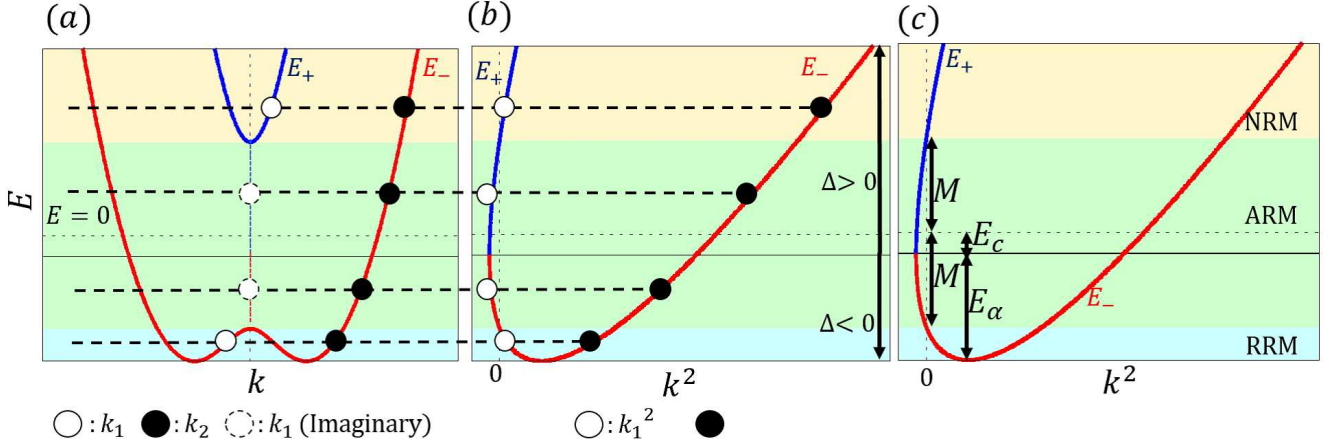


FIG. 3. (Color Online) Relation between the momentum of the transmitted wave function k_1 (open circle) and k_2 (closed circle) of each Fermi level (dashed line). (a) The energy dispersion of the FRM is plotted as a function of k . We find that in ARM (colored green region), k_1 takes pure imaginary (dashed closed circle). (b) The energy dispersion of the FRM plotted as a function of k^2 . It is noticed that $k_1^2 (< k_2^2)$ takes negative value in ARM of each Fermi level. Moreover, we find the wave function is changed at $\Delta = 0$ (bold line). (c) Relation among exchange coupling M , Rashba energy $E_\alpha = m^* \alpha^2 / (2\hbar^2)$, and $E_c = \hbar^2 M^2 / (2m^* \alpha^2)$. E_+ and E_- cross at $E = -E_c$.

$G = dI / (LdV)$, is given by

$$G = \frac{e^2}{4\pi^2 \hbar} \int_{-\pi/2}^{\pi/2} d\phi \cos \phi k_F \left[T^\uparrow(E_F, \phi) + T^\downarrow(E_F, \phi) \right]. \quad (13)$$

C. Results

Figure 4 shows the gate-voltage dependence of the tunneling conductance $G(V_g)$ in NM/FRM junction for several E_α at $Uk_F/E_F = 1.0$ with $k_F = \sqrt{2m^*E_F}/\hbar$. First, to clarify properties of $G(V_g)$, we consider a typical tunneling conductance G_{1D} (G_{2D}) in the absent of RSOC and magnetization in one (two)-dimensional NM/NM tunneling junction. In these junction, gate-voltage V_g are attached in a right-side of the junctions. Then, it is known that G_{1D} is independent of V_g except when the Fermi level is located far from the band bottom in the right-side. When the Fermi level is near the band bottom in the right-side, G_{1D} decrease rapidly with increasing the V_g . G_{2D} decreases monotonically [see inset in Fig. 4].

Second, we consider the obtained results. We find that, in NRM ($0 < eV_g/E_F < 0.5$), G decreases monotonically with increasing V_g , and its V_g -dependence is almost independent of E_α . Such a monotonic dependence is the same as that of G_{2D} . In ARM ($0.5 < eV_g/E_F < 1.5$), qualitative feature of the $G(V_g)$ depends on whether $2E_\alpha > M$ is satisfied or not. When the $2E_\alpha$ is smaller than the M ($2E_\alpha/E_F = 0.1$ in Fig. 4), the G decreases monotonically with increasing the V_g . This V_g -dependence is similar to that of G_{2D} . Here, $E_\alpha = m^* \alpha^2 / (2\hbar^2)$ is Rashba energy^{21,24,31,34-37} [see Fig. 3(c)]. On the other hand,

when $2E_\alpha > M$ is satisfied ($2E_\alpha/E_F = 1.1, 2.0$ in Fig. 4), G is almost independent of the V_g . This behavior is similar to that of G_{1D} . It is noted that there is no RRM for $2E_\alpha \leq M$, but RRM is realized for $2E_\alpha > M$. In RRM ($1.5 < eV_g/E_F$), the V_g -dependence of the G is similar to that of G_{1D} . Even in 2D junction, the conductance in ARM is 1D- (2D-) like for strong (weak) RSOC. In addition, in RRM, the V_g -dependence is similar to G_{1D} . Thus, by tuning Fermi level, the V_g -dependence of the conductance is dramatically changed. This is the main result in this work.

Figure 5(a), and (b) show the V_g -dependence of G for any strengths of the potential barrier: $Uk_F/E_F = 0, 1, 3$, in the presence of weak RSOC ($2E_\alpha < M$: $2E_\alpha/E_F = 0.1, M/E_F = 0.5$), and in strong RSOC ($2E_\alpha > M$: $2E_\alpha/E_F = 2.0, M/E_F = 0.5$). Both figures show that the V_g -dependence is qualitatively the same for any strengths of the potential barrier.

III. DISCUSSION

A. Ferromagnetic Rashba system

To qualitatively clarify the origin of the anomalous V_g -dependence of tunneling conductance in Sec. II, we consider the energy dispersion of the FRM. The energy dispersion becomes

$$E_\pm(k) = \frac{\hbar^2 k^2}{2m^*} \pm \sqrt{\alpha^2 k^2 + M^2} - (E_F - eV_g). \quad (14)$$

The dispersion can be classified into three cases: (i) $M = 0$, (ii) $0 < M < 2E_\alpha$, (iii) $M \geq 2E_\alpha$ as shown in Fig.

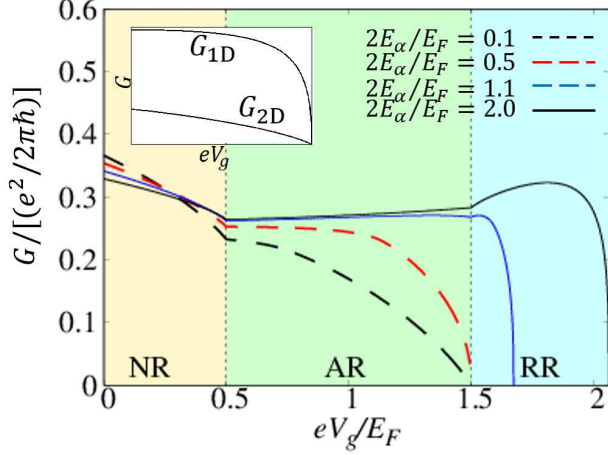


FIG. 4. (Color Online) V_g -dependence of G for several E_α at $M/E_F = 0.5$, and $Uk_F/E_F = 1.0$ with $k_F = \sqrt{2m^*E_F}/\hbar$. Here, E_α , M , and U are the Rashba energy, exchange coupling, and strength of the potential barrier. In this case, $2E_\alpha/E_F = 0.1, 0.5$, and $2E_\alpha/E_F = 1.1, 2.0$ shows the band structure of FRM in cases (iii), and (ii), respectively [see Fig. 1 (b)-(c)]. (inset) G_{1D} , and G_{2D} shows a typical tunneling conductance in a one-dimensional, and two-dimensional NM/NM junction. G_{1D} is almost independent of V_g except around the band bottom, and decreases rapidly with increasing the V_g when the Fermi level is located near the band bottom. G_{2D} decreases monotonically with increasing V_g .

1 (a)-(c). In case (i), RSOC lifts the spin degeneracy except for $k = 0$, and the energy dispersion splits into two branches. E_- branch has an annular minimum²¹ for $k = \sqrt{2m^*E_\alpha}/\hbar$. In case (ii), two branches perfectly split due to the presence of M . E_- branch has an annular minimum for $k = \sqrt{2m^*(E_\alpha - E_c)}/\hbar$, which is affected from E_c . In case (iii), E_- branch has a minimum at $\mathbf{k} = 0$.

The spin structure at Fermi surface depends on the position of Fermi level, due to the RSOC and M . As a result, three types of spin structures appear for NRM, ARM, and RRM [see Fig. 1(d)-(f)]. In NRM, there are two Fermi surfaces with opposite direction of spin³. In ARM, the inner Fermi surface disappears. In RRM, the spin structure in the inner and outer Fermi surface take the same spin structure.

B. Fermi surface and DOS

Since tunneling conductance basically reflects on the shape of Fermi surface, we consider Fermi surface in each state of FRM. We find that the Fermi surface in NRM is in the shape of disk, but the shape of the Fermi surface in RRM is a ring. Actually, the momentum-dependence of the Fermi surface of each states is given by changing Fermi energy dE_F . The derivative of Fermi surface dS

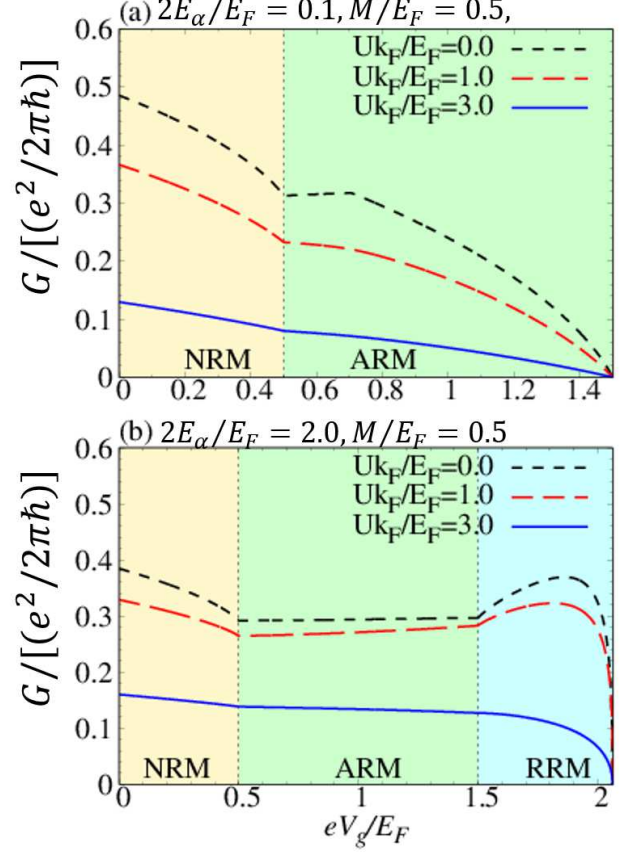


FIG. 5. (Color Online) V_g -dependence of G for several U with $M/E_F = 0.5$ in (a) weak RSOC ($2E_\alpha/E_F = 0.1$), and in (b) strong RSOC ($2E_\alpha/E_F = 2.0$). (a), and (b) correspond to the band structure of Fig. 1(b), and (c), respectively.

is described by infinitesimal change of the momentum k_1 and k_2 as

$$\begin{cases} dS = 2\pi(k_1 dk_1 + k_2 dk_2) & (\text{NRM}), \\ dS \sim 2\pi k_b d\tilde{k} & (\text{RRM}), \end{cases} \quad (15)$$

where $d\tilde{k} = dk_2 - dk_1$ is the infinitesimal change of \tilde{k} , and $\tilde{k} = k_2 - k_1$ is the width of the ring of the Fermi surface in RRM (see Fig. 6). Here, $k_b = \sqrt{2m^*(E_\alpha - E_c)}/\hbar$ is a constant of \mathbf{k} . From Eq. (15), we find that dS is proportional to $k_1 dk_1$ and $k_2 dk_2$. Hence, dS in NRM is the same as that in 2D-NM³⁸. On the other hand, dS in RRM is proportional to $d\tilde{k}$, and dS is equivalent to that in 1D-NM in the absence of RSOC and magnetization. In addition, it is natural to expect that dS in ARM is the mixture of that in 1D- and 2D-NM. These dS could reflect on the anomalous V_g -dependence of G , qualitatively.

Moreover, in order to phenomenologically understand the V_g -dependence of the G , we calculate DOS in each state in FRM by using Green's functions. Detail of the

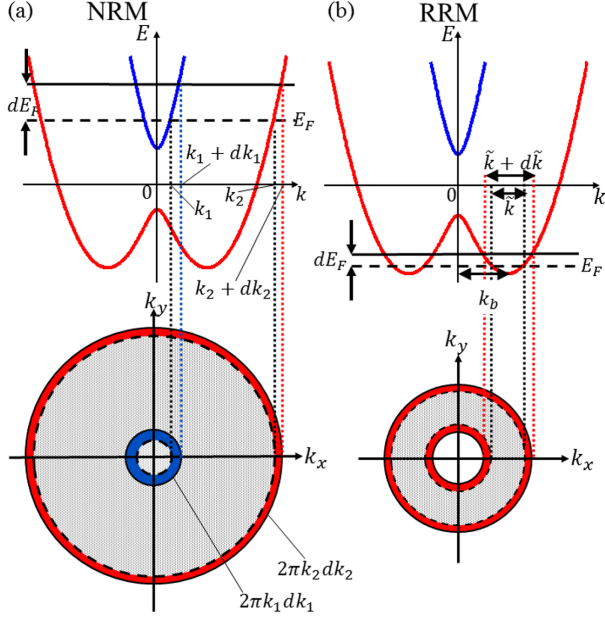


FIG. 6. (Color Online) Fermi surface in (a)NRM, and (b)RRM as a function of momentum. In Fig. (a), Red, and blue regions show the changed volume of the inner, and outer Fermi surface. $k_{1(2)}$ is the momentum of inner (outer) Fermi surface. In Fig. (b), Red regions show the changed volume of a ring for RRM. Here, \tilde{k} is the width of the ring, and $k_b = \sqrt{2m^*(E_\alpha - E_c)}/\hbar$ is constant. Dotted lines in the $k_x - k_y$ space denote the Fermi surface before the changing Fermi energy.

calculation is shown in Appendix. The DOS at the Fermi level, $\text{DOS}(E_F - eV_g)$, is analytically given by

$$\text{DOS}(E_F - eV_g) = \begin{cases} 2\nu_e & \text{(NRM),} \\ \nu_e \sqrt{\frac{E_\alpha}{\epsilon_F}} + \nu_e & \text{(ARM),} \\ 2\nu_e \sqrt{\frac{E_\alpha}{\epsilon_F}} & \text{(RRM).} \end{cases} \quad (16)$$

where $\nu_e = m^*/(2\pi\hbar^2)$ is the DOS in 2D-NM in the absence of RSCO and magnetization, $\epsilon_F = E_F - eV_g + E_\alpha + E_c$ is a liner function of $E_F - eV_g$. These results are plotted in Fig. 7 as a function of V_g for several E_α at $M/E_F = 0.5$. From the above equations, we find that in NRM ($eV_g/E_F < 0.5$), the conventional DOS, which is independent of the Fermi level, is obtained. In addition, the RSOC and magnetization does not affect the DOS in NRM. On the other hand, in ARM ($0.5 < eV_g/E_F < 1.5$) and RRM ($1.5 < eV_g/E_F$), the DOS depends on the Fermi level, which can be caused by the RSOC and magnetization. In particular, in RRM, the DOS is proportional to $1/\sqrt{\epsilon_F}$. Hence, the DOS in RRM is almost equivalent to that in one-dimensional electron gas (1DEG). In ARM, the DOS is composed of two parts. These parts can be regarded as DOS in two-dimensional electron gas (2DEG),

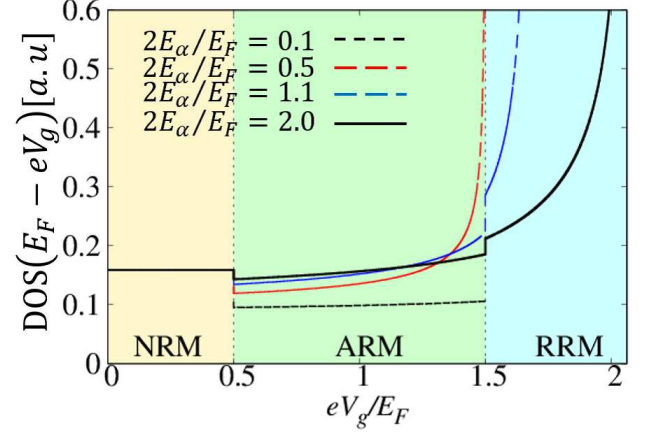


FIG. 7. (Color Online) V_g -dependence of the DOS in the two-dimensional FRM for several E_α at $M/E_F = 0.5$. V_g corresponds to the position of the Fermi level in FRM. The DOS in NRM is independent of RSOC and is exactly equal to that in 2DEG. The RSOC parameter $2E_\alpha/E_F < 1.0$ and $2E_\alpha/E_F > 1.0$ corresponds to cases (ii) and (iii), respectively [See Fig. 1]. In weak RSOC ($2E_\alpha/E_F = 0.1$) regime, the DOS is almost independent of eV_g , namely, position of the Fermi level, even in the ARM. However, in strong RSOC ($2E_\alpha \approx M$), the DOS in ARM and RRM depends on eV_g . In particular, the V_g -dependence of the DOS in the RRM is about equal to that in 1D-NM in the absence of the RSOC and exchange coupling.

and that in 1DEG, as shown in Eq. (16). Besides, we find that in weak RSOC ($2E_\alpha/E_F = 0.1$) region, the DOS tend to be like the DOS in 2DEG. In strong RSOC, the DOS is approximately equal to that in 1DEG. Thus, the energy dependence of the DOS is changed by V_g . In other words, the characteristic dimensionality can be seen from the V_g -dependence of the DOS.

In general, tunneling conductance is phenomenologically determined by the product of DOS in left-side and that in right-side of junction as^{26,27}

$$G(E_F) \sim \text{DOS}_L(E_F) \text{DOS}_R(E_F - eV_g), \quad (17)$$

where $\text{DOS}_{L(R)}$ is the bulk DOS in left- (right-) side of the junction. From the above equation, we consider the conductance discussed in Sec. III. Then, the DOS in NM in left-side of the junction becomes $\text{DOS}_L = 2\nu_e$ and is constant as a function of V_g . Hence, the tunneling conductance is qualitatively determined from $\text{DOS}_R(E_F - eV_g)$, as shown in Eq. (16). Therefore, the characteristic dimensionality of the DOS in FRM could directly reflect on the conductivity. The characteristic dimensionality of the DOS qualitatively agrees with the anomalous V_g -dependence of G .

IV. CONCLUSION

We theoretically study tunneling conductance $G(V_g)$ in two-dimensional NM/FRM junction, where the Fermi level of the FRM is tuned by the applied gate voltage (V_g). This paper focuses on the nontrivial metallic states in FRM, *i.e.*, NRM, ARM, and RRM, which are realized both in the presence of RSOC and magnetization. First, we find that in ARM, unique behavior of the V_g -dependence of G appears, due to the coexistence of RSOCs and exchange coupling M . The conductance strongly depends on the magnitude of the RSOC: In weak RSOC, $G(V_g)$ is equal to the V_g -dependence of the conventional tunneling conductance in the absence of RSOC and magnetization. However, in the presence of strong RSOC, $G(V_g)$ is almost independent of V_g . As a result, even in the two-dimensional system, the V_g -dependence is almost equivalent to that in 1DEG. Second, we obtain that V_g -dependence of G in RRM is similar to that in the conventional 1DEG. Such an anomalous V_g -dependence of $G(V_g)$ could be benefit from the characteristic dimensionality of the DOS of each the nontrivial metallic states. We expect that FRM has been realized in the thin heterostructure of Pt/Co/AlO_x reported recently. The RSOC can be caused by the inversion symmetry breaking along the layered direction and the exchange coupling comes from the Co film³⁹. By using the RSOC coefficient ($\alpha \approx 1\text{eV}\text{\AA}$)³⁹ and $\hbar^2/(2m^*) \approx 1\text{eV}\text{\AA}^2$, the Rashba energy is estimated as $E_\alpha \approx 0.1\text{eV}$. The magnitude of the exchange coupling could be estimated from the typical exchange coupling of ferromagnets, $M \sim 1\text{eV}$, since the magnetization of the thin heterostructure is similar to that of its bulk²⁸. Although its exchange coupling tends to be larger than the energy scale of the RSCO, the exchange coupling could be manipulated by an external magnetic field: The magnetic hysteresis of magnetization is manipulated by using an applied magnetic field and exchange coupling is proportional to the magnetization. Hence, the exchange coupling M could be manipulated by an applied magnetic field. Therefore, we expect that, in the heterojunction with applying magnetic field along the out-of-plane direction, a situation of $2E_\alpha > M$ can be experimentally realized by using property of the magnetic hysteresis. Moreover, we note that a thin film heterojunction could be reasonable for substantially tuning the Fermi level by means of gate-voltage. Finally, we expect that the origin of the obtained results lie on the spin-momentum locking rather than the characteristic dimensionality of the DOS in the nontrivial metallic states in FRM. Therefore, these results can open the next-generation of the field of the spintronics via both strong RSOCs and magnetism.

ACKNOWLEDGMENTS

We would like to thank K. Yada and K.T. Law for valuable discussion. This work was supported by a

Grant-in-Aid for Scientific Research on Innovative Areas, Topological Material Science (Grants No. JP15H05851, No. JP15H05853 No. JP15K21717), a Grant-in-Aid for Challenging Exploratory Research (Grant No. JP15K13498) from the Ministry of Education, Culture, Sports, Science, and Technology, Japan (MEXT), the Core Research for Evolutional Science and Technology (CREST) of the Japan Science and Technology Corporation (JST)(Grants No. JPMJCR14F1).

Appendix A: Derivation of the density of states

We show the detailed derivation of DOS in FRM [see Eq. (16)]. The spin-dependent DOS is defined by

$$\rho(E'_F) \equiv -\frac{1}{\pi} \text{Im} \sum_{\mathbf{k}} \mathcal{G}_{\mathbf{k}}^R(E'_F), \quad (\text{A1})$$

where $E'_F = E_F - eV_g$ corresponds to the position of the Fermi surface. $\mathcal{G}_{\mathbf{k}}^R(E'_F) \equiv (E'_F - H_{FRM} + i\delta)^{-1}$ is the retarded Green's function, and δ is an infinitesimal positive value. From Eq. (A1), we find that the off-diagonal components are zero ($\rho_{\uparrow\downarrow} = \rho_{\downarrow\uparrow} = 0$) in every case. The retarded Green's function can be divided into two parts as follow;

$$\mathcal{G}_{\mathbf{k}}^R = \mathcal{G}_{\mathbf{k}}^{R+} + \mathcal{G}_{\mathbf{k}}^{R-}, \quad (\text{A2})$$

where

$$\mathcal{G}_{\mathbf{k}}^{R\pm} = \frac{\Omega_{\pm}}{E'_F - E_{\pm} + i\delta}, \quad (\text{A3})$$

$$\Omega_{\pm} = \frac{1}{2}(1 \pm \mathbf{n} \cdot \boldsymbol{\sigma}), \quad (\text{A4})$$

$$\mathbf{n} \equiv -\frac{\alpha(\mathbf{k} \times \hat{\mathbf{z}}) + M\hat{\mathbf{z}}}{\sqrt{\alpha^2 k^2 + M^2}}. \quad (\text{A5})$$

Here, $\hat{\mathbf{z}}$ is a unit vector along z -axis. $\mathcal{G}_{\mathbf{k}}^{R\pm}$ are the Green's function of E_{\pm} . Therefore, Eq. (A1) is decomposed as follow;

$$\rho(E'_F) = \rho^+(E'_F) + \rho^-(E'_F), \quad (\text{A6})$$

$$\rho^{\pm}(E'_F) \equiv -\frac{1}{\pi} \text{Im} \sum_{\mathbf{k}} \mathcal{G}_{\mathbf{k}}^{R\pm}(E'_F). \quad (\text{A7})$$

We calculate $\rho^-(E'_F)$.

$$\begin{aligned} \rho^-(E'_F) &= -\frac{1}{2\pi} \text{Im} \sum_{\mathbf{k}} \frac{1 - \mathbf{n} \cdot \boldsymbol{\sigma}}{E'_F - E_- + i\delta} \\ &= -\frac{1}{4\pi^2} \text{Im} \int_0^\infty k dk \frac{1 - n_z \sigma_z}{E'_F - E_- + i\delta} \\ &= \frac{v_e}{2\pi} \text{Im} \int_0^\infty d\epsilon_0 \frac{1 - n_z(\epsilon_0) \sigma_z}{\epsilon_0 - 2\sqrt{E_\alpha} \sqrt{\epsilon_0 + E_c} - (E'_F + i\delta)}, \end{aligned} \quad (\text{A8})$$

where $\epsilon_0 = \hbar^2 k^2 / (2m^*)$ is the kinetic energy in NM. We set $\xi = \sqrt{\epsilon_0 + E_c}$. ρ^- becomes

$$\rho^-(E'_F) = \frac{\nu_e}{\pi} \text{Im} \int_{\sqrt{E_c}}^{\infty} d\xi \frac{[1 - n_z(\xi)\sigma_z]\xi}{\xi^2 - 2\sqrt{E_\alpha}\xi - (E'_F + E_c) - i\delta}. \quad (\text{A9})$$

n_z is given by

$$n_z = -\frac{M}{\sqrt{\alpha^2 k^2 + M^2}} = -\sqrt{\frac{E_c}{\epsilon_0 + E_c}} = -\frac{\sqrt{E_c}}{\xi}. \quad (\text{A10})$$

As a result, we can obtain

$$\begin{aligned} \rho^-(E'_F) &= \frac{\nu_e}{\pi} \text{Im} \int_{\sqrt{E_c}}^{\infty} d\xi \frac{\xi + \sqrt{E_c}\sigma_z}{F_-(\xi) - i\delta} \\ &= \frac{\nu_e}{2i\pi} \int_{\sqrt{E_c}}^{\infty} d\xi \left[\frac{\xi + \sqrt{E_c}\sigma_z}{F_-(\xi) - i\delta} - \frac{\xi + \sqrt{E_c}\sigma_z}{F_-(\xi) + i\delta} \right] \\ &= \nu_e \int_{\sqrt{E_c}}^{\infty} d\xi (\xi + \sqrt{E_c}\sigma_z) \delta[F_-(\xi)]. \end{aligned} \quad (\text{A11})$$

Here, $F_-(\xi)$ is expressed by

$$F_-(\xi) = \xi^2 - 2\sqrt{E_\alpha}\xi - (E'_F + E_c) = (\xi - \xi_1)(\xi - \xi_2), \quad (\text{A12})$$

with $\xi_{1(2)} = \sqrt{E_\alpha} + (-)\sqrt{\epsilon_F}$, and $\epsilon_F = E_F - eV_g + E_\alpha + E_c$. Then, $\delta[F_-(\xi)]$ in Eq. (A11) is estimated by;

$$\begin{aligned} \delta[F_-(\xi)] &= \frac{1}{|\partial_\xi F_-(\xi_1)|} \delta(\xi - \xi_1) + \frac{1}{|\partial_\xi F_-(\xi_2)|} \delta(\xi - \xi_2) \\ &= \frac{1}{2\sqrt{\epsilon_F}} [\delta(\xi - \xi_1) + \delta(\xi - \xi_2)]. \end{aligned} \quad (\text{A13})$$

As a result, we have

$$\begin{aligned} \rho^-(E'_F) &= \frac{\nu_e}{2\sqrt{\epsilon_F}} \int_{\sqrt{E_c}}^{\infty} d\xi (\xi + \sqrt{E_c}\sigma_z) \\ &\quad \times [\delta(\xi - \xi_1) + \delta(\xi - \xi_2)] \\ &= \frac{\nu_e}{2} \left[\left(1 + \frac{2E_\alpha + M\sigma_z}{2\sqrt{E_\alpha}\epsilon_F} \right) \theta(\sqrt{\epsilon_F} + \sqrt{E_\alpha} - \sqrt{E_c}) \right. \\ &\quad \left. + \left(-1 + \frac{2E_\alpha + M\sigma_z}{2\sqrt{E_\alpha}\epsilon_F} \right) \theta(-\sqrt{\epsilon_F} + \sqrt{E_\alpha} - \sqrt{E_c}) \right]. \end{aligned} \quad (\text{A14})$$

To replace $\sqrt{E_\alpha}$ with $-\sqrt{E_\alpha}$, we obtain ρ^+ as follow:

$$\rho^+(E'_F) = \frac{\nu_e}{2} \left(1 - \frac{2E_\alpha + M\sigma_z}{2\sqrt{E_\alpha}\epsilon_F} \right) \theta(\sqrt{\epsilon_F} - \sqrt{E_\alpha} - \sqrt{E_c}). \quad (\text{A15})$$

From Eqs. (A15) and (A14), we can obtain the spin-dependent DOS $\rho(E'_F)$ as follow:

$$\begin{aligned} \rho(E'_F) &= \frac{\nu_e}{2} \left[\left(1 - \frac{2E_\alpha + M\sigma_z}{2\sqrt{E_\alpha}\epsilon_F} \right) \theta(\sqrt{\epsilon_F} - \sqrt{E_\alpha} - \sqrt{E_c}) \right. \\ &\quad \left. + \left(1 + \frac{2E_\alpha + M\sigma_z}{2\sqrt{E_\alpha}\epsilon_F} \right) \theta(\sqrt{\epsilon_F} + \sqrt{E_\alpha} - \sqrt{E_c}) \right. \\ &\quad \left. + \left(-1 + \frac{2E_\alpha + M\sigma_z}{2\sqrt{E_\alpha}\epsilon_F} \right) \theta(-\sqrt{\epsilon_F} + \sqrt{E_\alpha} - \sqrt{E_c}) \right]. \end{aligned} \quad (\text{A16})$$

Here, the resulting DOS as Eq. 16 is given by $\text{Tr}[\rho] = \rho_{\uparrow\uparrow} + \rho_{\downarrow\downarrow}$ in case(ii). The DOS in case (i)-(iii) are shown in Table. II). We can demonstrate the DOS in M=0 agrees with that in Ref. 24.

TABLE II. V_g -dependence of the DOS in the Fermi surface of FRM for NRM, ARM, and RRM in case (i)-(iii). The position of the Fermi level becomes lower with increasing V_g . Here, $\epsilon_F = E_F - eV_g + E_\alpha + E_c$ is a liner function of $E_F - eV_g$, and ν_e is the DOS in 2DEG. NRM, ARM, and RRM is realized in $0 < eV_g < E_F - M$, $E_F - M < eV_g < E_F + M$, and $E_F + M < eV_g < E_F + E_\alpha + E_c$, respectively.

| Case | NRM | ARM | RRM |
|--------------------------|----------|--|---|
| (i) $M = 0$ | $2\nu_e$ | - | $\nu_e(2\sqrt{E_\alpha}/\sqrt{\epsilon_F})$ |
| (ii) $0 < M < 2E_\alpha$ | $2\nu_e$ | $\nu_e[1 + \sqrt{E_\alpha}/\sqrt{\epsilon_F}]$ | $\nu_e(2\sqrt{E_\alpha}/\sqrt{\epsilon_F})$ |
| (iii) $M \geq 2E_\alpha$ | $2\nu_e$ | $\nu_e[1 + \sqrt{E_\alpha}/\sqrt{\epsilon_F}]$ | - |

¹ D. Grundler, Phys. Rev. B **63**, 161307 (2001).

² M. H. Larsen, A. M. Lunde, and K. Flensberg, Phys. Rev. B **66**, 033304 (2002).

³ P. Středa and P. Šeba, Phys. Rev. Lett. **90**, 256601 (2003).

⁴ O. Krupin, G. Bihlmayer, K. Starke, S. Gorovikov, J. Prieto, K. Döbrich, S. Blügel, and G. Kaindl, Phys. Rev. B **71**, 201403 (2005).

⁵ D. Sánchez, L. Serra, and M.-S. Choi, Phys. Rev. B **77**, 035315 (2008).

⁶ V. Fallahi and M. Ghanaatshoar, Phys. Status Solidi (B) **249**, 1077 (2012).

⁷ M. Pang and C. Wang, Phys. E: Low-dimensional Systems and Nanostructures **44**, 1636 (2012).

⁸ C.-S. Tang, S.-Y. Chang, and S.-J. Cheng, Phys. Rev. B **86**, 125321 (2012).

- ⁹ C.-S. Tang, J.-A. Keng, N. R. Abdullah, and V. Gudmundsson, arXiv:1612.05899 (2016).
- ¹⁰ T. Fukumoto, K. Taguchi, S. Kobayashi, and Y. Tanaka, Phys. Rev. B **92**, 144514 (2015).
- ¹¹ S. Han, L. Serra, and M.-S. Choi, J. Phys: Cond. Mat. **27**, 255002 (2015).
- ¹² P. Wójcik, J. Adamowski, M. Wołoszyn, and B. Spisak, J. Appl. Phys. **118**, 014302 (2015).
- ¹³ T. Yokoyama, Y. Tanaka, and N. Nagaosa, Phys. Rev. B **81**, 121401 (2010).
- ¹⁴ S. Mondal, D. Sen, K. Sengupta, and R. Shankar, Phys. Rev. Lett. **104**, 046403 (2010).
- ¹⁵ K. Taguchi, T. Yokoyama, and Y. Tanaka, Phys. Rev. B **89**, 085407 (2014).
- ¹⁶ L. W. Molenkamp, G. Schmidt, and G. E. Bauer, Phys. Rev. B **64**, 121202 (2001).
- ¹⁷ T. Matsuyama, C.-M. Hu, D. Grundler, G. Meier, and U. Merkt, Phys. Rev. B **65**, 155322 (2002).
- ¹⁸ Y. Jiang and M. Jalil, J. Phys: Cond. Mat. **15**, L31 (2003).
- ¹⁹ V. M. Ramaglia, D. Bercioux, V. Cataudella, G. D. Filippis, C. Perroni, and F. Ventriglia, Eur. Phys. J. B-Condensed Matter and Complex Systems **36**, 365 (2003).
- ²⁰ T. Yokoyama, Y. Tanaka, and J. Inoue, Phys. Rev. B **74**, 035318 (2006).
- ²¹ B. Srisongmuang, P. Pairor, and M. Berciu, Phys. Rev. B **78**, 155317 (2008).
- ²² A. Matos-Abiague and J. Fabian, Phys. Rev. B **79**, 155303 (2009).
- ²³ P. Zhang and M. Xu, Sci. China Phys., Mechanics and Astronomy **56**, 1514 (2013).
- ²⁴ A. Jantayod and P. Pairor, Phys. E: Low-dimensional Systems and Nanostructures **48**, 111 (2013).
- ²⁵ A. Jantayod and P. Pairor, Superlattices and Microstructures **88**, 541 (2015).
- ²⁶ M. B. Stearns, J. Magn. Magn. Mater. **5**, 167 (1977).
- ²⁷ S. Maekawa and U. Gafvert, IEEE. Trans. Magn **18**, 707 (1982).
- ²⁸ I. M. Miron, G. Gaudin, S. Auffret, B. Rodmacq, A. Schuhl, S. Pizzini, J. Vogel, and P. Gambardella, Nat. Mater **9**, 230 (2010).
- ²⁹ S. Datta and B. Das, Appl. Phys. Lett. **56**, 665 (1990).
- ³⁰ E. I. Rashba, Sov. Phys. Solid State **2**, 1109 (1960).
- ³¹ J. Cayao, E. Prada, P. San-Jose, and R. Aguado, Phys. Rev. B **91**, 024514 (2015).
- ³² U. Zülicke and C. Schroll, Phys. Rev. Lett. **88**, 029701 (2001).
- ³³ Y. Meir and N. S. Wingreen, Phys. Rev. Lett. **68**, 2512 (1992).
- ³⁴ C. R. Ast, J. Henk, A. Ernst, L. Moreschini, M. C. Falub, D. Pacilé, P. Bruno, K. Kern, and M. Grioni, Phys. Rev. Lett. **98**, 186807 (2007).
- ³⁵ C. R. Ast, D. Pacilé, L. Moreschini, M. C. Falub, M. Pagnano, K. Kern, M. Grioni, J. Henk, A. Ernst, S. Ostanin, *et al.*, Phys. Rev. B **77**, 081407 (2008).
- ³⁶ S. Mathias, A. Ruffing, F. Deicke, M. Wiesenmayer, I. Sakar, G. Bihlmayer, E. Chulkov, Y. M. Koroteev, P. Echenique, M. Bauer, *et al.*, Phys. Rev. Lett. **104**, 066802 (2010).
- ³⁷ K. Ishizaka, M. Bahramy, H. Murakawa, M. Sakano, T. Shimojima, T. Sonobe, K. Koizumi, S. Shin, H. Miyahara, A. Kimura, *et al.*, Nat. Mater **10**, 521 (2011).
- ³⁸ To consider k_1 and k_2 as the functions of E_F , both $k_1 dk_1$ and $k_2 dk_2$ include the 1D-like term proportional to $1/\sqrt{\epsilon_F}$ with $\epsilon_F = E_F - V_g + E_\alpha + E_c$. However, these 1D-like terms have different signs in each other, and cancel out in the sum of dS .
- ³⁹ It is noted that the strong RSOC ($\alpha \sim 1\text{eV\AA}$) has been reported in heavy-metal systems^{34,36,37}, and its Rashba energy is estimated $E_\alpha \sim 0.1\text{eV}$. To attach a ferromagnet on these materials, it is expected that FRM becomes realized.